J. Hydrol. Hydromech., 74, 2026, 1, 20–35
https://doi.org/10.2478/johh-2026-0003

Journal of Hydrology and Hydromechanics

Scour evolution for steady and unsteady flow conditions downstream of Type A piano key weirs

Manisha Panthi[1], Brian Mark Crookston[1*], Michele Palermo[2]

[1] Utah Water Research Laboratory, Dept. of Civil and Env. Engineering, Utah State University, 8200 Old Main Hill, Logan, UT 84322-8200 USA.
[2] DESTEC- Department of Energy, Systems, Territory and Construction Engineering, University of Pisa, Via Gabba 22, 56122 Pisa, Italy.
[*] Corresponding author. E-mail: brian.crookston@usu.edu

Abstract: For the first time a comprehensive analysis for steady and unsteady flow conditions was performed of time-dependent scour processes in non-cohesive sediment downstream of a Type A piano key weir. The evolution and progression of scour of large-scale laboratory experiments were interpreted using an empirical approach and adapting a theoretical model based on the phenomenological theory of turbulence developed elsewhere. The results were within 30% of experimental with the R-squared values of 0.972 for the theoretical model and 0.993 for a calibrated empirical model. Results of this study demonstrate consistent scour evolution kinetics between steady and unsteady flow cases, although in the latter, the maximum scour features were smaller than their steady-state counterparts. This study highlights the novelty of integrating experimental and theoretical frameworks to validate and enhance the design of complex hydraulic structures. Quantitative findings confirm the robustness of first principles-based approaches, offering practical insights and design parameters critical for addressing scour challenges in non-cohesive sediment environments.

Keywords: Temporal scour evolution; Non-cohesive sediment; Scour equilibrium; Stepped flood hydrograph; Unsteady flows.

1 INTRODUCTION

Hydraulic structures of many geometries and materials have been constructed in rivers and waterways for flood regulation, water diversion and conveyance, habitat support and ecosystem restoration, recreation, and to control river morphological processes (Erpicum et al., 2020; Ettema et al., 2004; Hager and Boes, 2014; Knight, 2013; Pagliara and Kurdistani, 2017; Rosgen, 2012; Schleiss, 2017; de Vriend et al., 2015). Hydraulic performance considerations may include watershed and river reach characteristics at multiple time scales, river connectivity and adjacent flow fields, energy dissipation, and structure stability (Chanson and Felder, 2017; Copeland et al., 2001; Hager et al., 2020; Novak et al., 2017). Scour at the structure toe remains a common design consideration and unfortunately a source of major damage that at times have resulted in incidents and failures (Melville, 2014). Risks associated with scour are generally increasing in part due to climate shifts evidenced by increasing storm duration and intensities and flood-drought cycles (Bermúdez et al., 2021; Cea and Costabile, 2022; Wasko et al., 2021). Thus, the consideration of scour should include flood estimation guidance for a variety of scenarios, including extreme floods and corresponding flood hydrographs.

Indeed, scour at the toe of various specific hydraulic structures (of both natural materials and concrete) has been widely analyzed for steady state conditions (Bormann and Julien, 1991; D'Agostino and Ferro, 2004; Dey and Sarkar, 2006; Ettema et al., 2004; Guan et al., 2015; Hoffmans and Pilarczyk, 1995; Jüstrich et al., 2016; Pagliara and Palermo, 2008; Pagliara et al., 2008; Pagliara and Kurdistani, 2013; Palermo and Pagliara, 2017) including scour development phases (Hoffmans and Verheij, 1997), evolution processes (Ben Meftah and Mossa, 2006) and scour design guidance (Burns et al., 2010; Ettema et al., 2011; Hoffmans and Verheij, 1997). The majority of scour studies or estimation of toe scour are assessed under steady flow conditions instead of unsteady flow conditions. In many river catchments, a flood hydrograph deviates from the steady-state considerations as discharges causing scour last for a finite (and often shorter) duration that may be affected by the rising and falling limbs of the hydrograph and any hysteresis effects.

One specific hydraulic structure, the piano key weir (PKW), is being regularly incorporated into river flood rehabilitation projects (Crookston et al., 2019). Limited exploration in the field of scour has been performed (see Table A1 in Appendix 1). Although there are different geometries, the Type A is the most common (Fig. 1); it features a crest (rectangular in plan) with wall segments parallel and perpendicular to the structure axis; these elements or keys also feature, in streamwise profile, ramps to guide flow towards and away from the control section thereby enhancing the spillway capacity with a significantly increased crest length and flow capacity for a given upstream river stage (Anderson and Tullis, 2012; Crookston et al., 2018; Leite Ribeiro et al., 2012; Lempérière and Ouamane, 2003; Machiels et al., 2011). However, these conveyance benefits translate to increased forces at the PKW toe that may exceed the erosive resistance of riverbed materials.

Jüstrich et al. (2016) is perhaps the first study to consider downstream scour for PKW and provided for the steady-state case a technique to estimate the equilibrium scour depth dimensions for gravel and sands. Palermo et al. (2020) investigated scour morphology of PKW, relating the scour depth to steady-state flow conditions, weir height and tailwater depth. Yazdi et al. (2020) also studied, for steady state conditions, the effect of PKW on equilibrium bed morphology, finding that a rectangular PKW causes deeper scour. Kumar and Ahmad (2022) and Lantz et al. (2022) also performed steady-state tests

with PKWs using gravel materials to study downstream scour profiles.

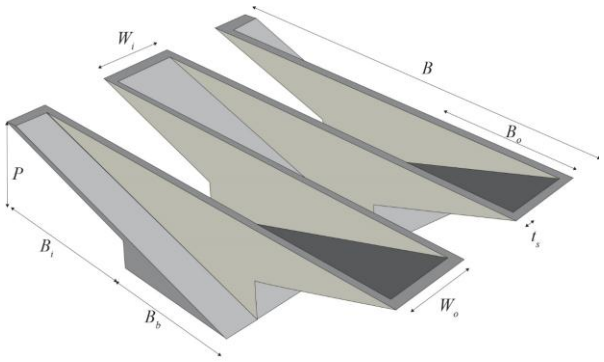

Fig. 1. Sketch of a typical Type A PKW.

Such approaches typically provide empirical, predicting equations derived via dimensional analysis and calibrated with experimental data (see Table A1 in Appendix 1). However, their validity is limited to the tested conditions. Conversely, theoretical methods are based on first principles, thus a potential to overcome/minimize these issues (Hoffmans, 2009). Among others, a theoretical approach for estimating scour depth at equilibrium was proposed by Bombardelli and Gioia (2006) and Gioia and Bombardelli (2005), using the phenomenological theory of turbulence (PTT). Such method was further implemented by Bombardelli et al. (2018), who considered the temporal scour evolution for vertical/sub-vertical jet-driven scour processes. It was found that the kinetics of the scour for both two- and three-dimensional scour configurations can be well represented via ordinary differential equations, relating the rate of scour depth to the characteristics of the bed material and flow conditions. The approach was further corroborated by the findings of Di Nardi et al. (2021) pertain to scour analysis downstream of different drop structures under steady flow conditions. As for the unsteady flow conditions, the methodology was initially adopted by Di Nardi et al. (2022), who applied it to jet scour and, successively, extended by Di Nardi et al. (2023) to the scour evolution of different hydraulic structures (e.g., bed sills, rock sills, stepped gabion weirs, and grade control weirs). In doing so, the authors highlighted the necessity of additional investigations for other structure typologies under different flow conditions.

For non-gated structures like PKW with passively controlled discharge, it is recommended that the time-dependent scour processes be considered, especially for a flood hydrograph scenario. While the maximum equilibrium scour features are typically studied under steady flow conditions, these studies might not accurately replicate the natural unsteady scour processes. In fact, an overestimate of the extent of scour is likely, as the naturally occurring flood event might not have sufficient duration compared to the steady flow equilibrium state (Di Nardi et al., 2023; Lança, 2013; Palermo and Pagliara, 2017). The conservative assumption derived by applying steady formulas may lead to cost increase. Therefore, predicting the evolution of toe scour over time during a flood event is essential and offers valuable insights for designers.

However, research on such predictions, particularly for structures with complex flow properties like PKWs is limited. Therefore, for the first time, this work aims at providing a comprehensive analysis of the time-dependent scour mechanism in non-cohesive sediment downstream of a Type A PKW, for steady and unsteady flow conditions. The research integrates large-scale laboratory experiments and scour theory, addressing the following key questions:

- How is scour kinetics influenced by a stepped hydrograph including peak discharge and incremental changes in discharge as a function of time?
- How does scour morphology from both steady and unsteady flow conditions at a PKW compare?
- Is the PTT-approach suitable to describe both the equilibrium features of the scour and its kinetics for steady and unsteady conditions?

To this end, the scour evolution downstream of PKWs was described under different hydraulic conditions and for both steady and unsteady cases. This includes insights into the physics of the phenomenon, highlighting the peculiar characteristics of the flow originating from this structure typology. Next, it is demonstrated that the basic assumptions of the PTT are reasonably corroborated by experimental evidence for the analyzed structures. Finally, it is shown that both equilibrium state and the temporal evolution of scour is adequately predicted by the PTT-approach, regardless of the inflow conditions and bed material characteristics.

2 METHODS

2.1 Experimental setup

This study includes clear-water physical experiments using a type A PKW with a non-cohesive movable bed, carried out at the Utah Water Research Laboratory in a 2 m wide, 1.8 m deep and 16 m long flume. The general experimental setup is shown in Fig. 2; it is an idealized or simplified scenario representing an in-channel weir with erodible sediment downstream. The PKW was placed 2.31 m from the flume headbox that was equipped with a diffuser to allow uniform flow conditions and a smooth entry of incoming flow. A 0.42 m tall Type A PKW (Table 1) was placed on a fixed substructure to approximate an approaching river channel and accommodate the alluvial bed. This alluvial bed was located immediately downstream of the PKW and was 2 m wide, 1 m deep, and 5 m long. The alluvial bed surface was planar and leveled with the base of the PKW for each test. It was made of a non-cohesive small gravel material with median grain size d_{50} = 6.5 mm, coefficient of gradation σ = 1.3 and specific density G = 2.65. Further details are provided in Panthi (2025a).

As shown in Fig. 2, h_u and h_d are the upstream and downstream head and ΔH is the energy head. Z_{max}, L_{max} and X_{max} are the maximum/equilibrium scour depth, length and location of maximum depth with Z, L and X being the scour depth, length and location of scour at an instant. The cartesian coordinates are x and z in the streamwise and vertical directions, with downward being positive. P_d is the height of the PKW platform. Please note that for this study the upstream conditions were negligible on scour and were formulated to have idealized approach conditions, where in the field certain conditions may lead to deposition upstream of the PKW (see Panthi 2025a). Discharges supplied to the facility head box were manually controlled using a large butterfly valve and measured using calibrated venturi meters (±0.25% accuracy). Upstream water levels were measured using a stilling well with a point gauge (±1.5 mm precision) and an ultrasonic sensor (Microsonic mic+130/IU/TC, ±1 % accuracy). Downstream water levels were a free flow condition measured with an identical ultrasonic sensor located in the channel.

Table 1. Parameters of the Type A PKW.

Parameter	Description	Value	Parameter	Description	Value
P	Height of weir	0.42 m	W_u	Width of a unit cycle	0.49 m
P_d	Depth of footing	1.09 m	W_i	Width of inlet key	0.26 m
B	Total longitudinal width of weir	1.04 m	W_i/W_o	Ratio of inlet to outlet key width	1.28
B_b	Width of PKW base	0.52 m	W	Width of weir	2 m
B_o	Overhang length of outlet key	0.26 m	t_s	Thickness of weir	0.025 m
B_i	Overhang length of inlet key	0.26 m	N	Number of cycles	4
L_c	Length of weir crest	10.16 m	L_c/W	Ratio of length of weir crest to width	5.08

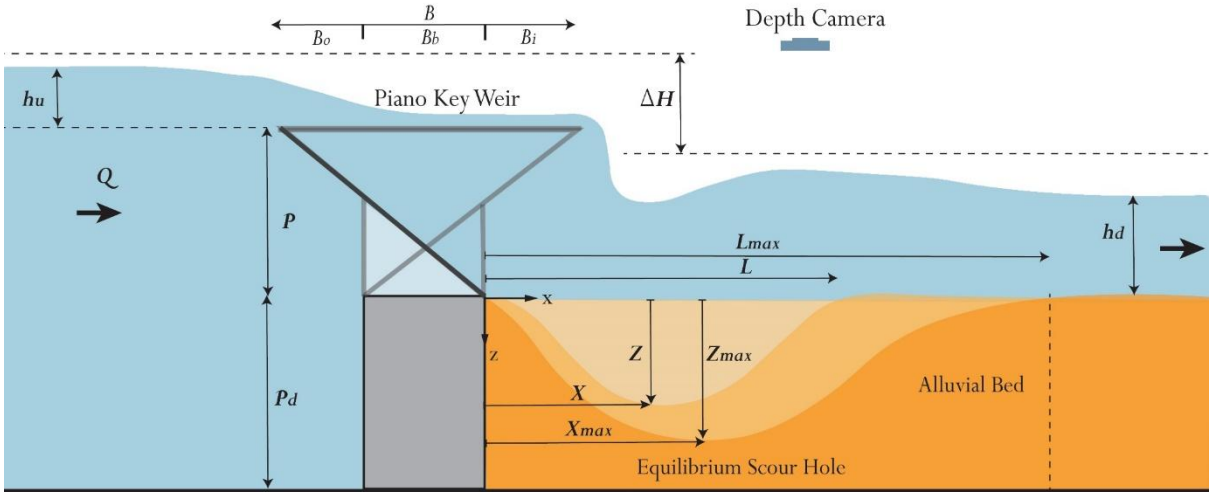

Fig. 2. Diagram sketch of the experimental apparatus along with the main geometric and hydraulic parameters.

Discharges supplied to the facility head box were manually controlled using a large butterfly valve and measured using calibrated venturi meters (±0.25% accuracy). Upstream water levels were measured using a stilling well with a point gauge (±1.5 mm precision) and an ultrasonic sensor (Microsonic mic+130/IU/TC, ±1 % accuracy). Downstream water levels were a free flow condition measured with an identical ultrasonic sensor located in the channel.

Scour evolution for instantaneous scour data were tracked in a large grided viewing window using marking stickers with annotations along with GoPro Hero 10 camera recordings capturing temporal data. Additionally, at the end of each experiment, bed profiles were surveyed via a point gauge system (±1.5 mm) using a carriage for longitudinal profile at the flume axis and cross-sectional profile was taken at Z_{max} location to observe variation of scour depths at inlet and outlet keys. In addition, a scanning system using an Intel Realsense D455 depth camera (±2%) was employed to capture images with depth information.

It is worth remarking that the adopted experimental apparatus allowed us to minimize scale effects, even though the experiments are not a scaled model with a specific geometric scale length ratio. A potential range of scales based upon the weir height would be about 1:2 to 1:14 (Crookston et al. 2019). According to Heller (2011), for in-stream hydraulic structures, such effects become negligible if the model scale is greater than 1:40. Furthermore, considering that the width of the model is 2 m and could represent an idealized section of a river, our results can be reasonably extended to prototype applications in natural streams/rivers whose width is less than 80 m, which represents the most common scenario for such structure typology. In order to consider scaling of the tested substrate and scour response, we refer readers to the Erodibility Index Method (Annandale 1995) that is commonly used in the USA as simply scaling grain diameters may not fully account for the scaling of incipient motion conditions and general scour processes between a laboratory experiment and the field.

2.2 Hydrographs and test scenarios

As noted, a novel aspect of this study is the inclusion of both steady-state and hydrograph scour testing. Expanding upon the steady-state flow tests performed by Lantz et al. (2022), which was simulated until negligible variation of the bed configuration occurred, studies with inflow hydrograph focusing on two discharge (Q) cases of 600 l/s and 300 l/s were conducted. Synthetic hydrographs were simulated in the laboratory by incremental adjustments with the supply pipeline valve, producing the desired stepped shape for different peak discharges, Q_{peak} (Brunner et al., 2017; Di Nardi et al., 2023; Mediero et al., 2010; Phillips et al., 2018). Hydrograph formulation adopted a stepped idealization with incremental changes in discharge and time (ΔQ and Δt, respectively) and considered in multiple cases from actual river flows; it was observed that in rivers with bigger catchment areas, more tributaries and storage effects have longer duration of falling limb like those characterizing rivers such as the Colorado River, Mississippi River, and Columbia River. Keeping the key hydrograph characteristics from actual rivers, we assumed that the number of steps in the falling limb were twice that of the rising counterpart. Hence, the shapes were simplified and further formulated to also have a direct comparison of results with unsteady flow effects on other low head structures (Di Nardi et al., 2023; Palermo and Pagliara, 2017).

Different hydrographs were simulated by varying the number of the steps n in the increasing phase, the total duration $t^* = (3n\text{-}1)\Delta t$ and the peak discharge $Q_{peak} = n\Delta Q_i$, with Δt and ΔQ_i indicating the duration and the discharge increment of each i-step

of the rising limb. (Note that, for the falling limb, Δt was the same as the rising limb and the discharge decrement was equal to $0.5\Delta Q_i$). In order to compare tests conducted under both steady and unsteady flow conditions, we followed the approach developed by Palermo and Pagliara (2017) for stepped gabion weirs and rock sills. Namely, for such structure configurations, the authors showed that, under unsteady flow conditions characterized by the same value of Q_{peak}, the differences in terms of the maximum scour depth become negligible provided time to peak $t_{peak} \geq t^*_{peak}$ with $n \geq 5$ and t^*_{peak} given by the following Eq. (1):

$$t^*_{peak} = \frac{T^*_{peak}\, h_c\, n}{\left[g\left(\frac{(\rho_s-\rho)}{\rho}\right)d_{50}\right]^{0.5}} \quad (1)$$

where h_c is the critical flow depth, and $T^*_{peak} \approx 3200$ and is a non-dimensional time. In this study, three values of n (i.e., 3, 6 and 9) were selected to simulate different hydrographs and analyze their sensitivity. An example of synthetic hydrograph with $n = 3$ in the rising limb is shown in the Fig. 3, i.e., the non-dimensional discharge Q/Q_{peak} is plotted as function of the non-dimensional time t/t^*, with Δt indicating the time duration of each increment/decrement of discharge. Similarly, we conducted tests under different durations of the incremental step Δt ranging from 12.33 to 58 minutes (Table 2). In other words, different times to peak mt^*_{peak} were selected creating a prolonged hydrograph with the same peak discharge, with m = 1, 1.5 and 2 indicating a multiplicative factor. Some examples of simulated hydrographs with $n = 6$ and different values of m are shown in Fig. 4. The test scenarios are named with nomenclature $Q_{peak}\_n\_m$ where Q_{peak} signifies the peak discharge, n signifies the number of steps in rising limb and m signifies the multiplier of t^*_{peak} used in the test (Table 2).

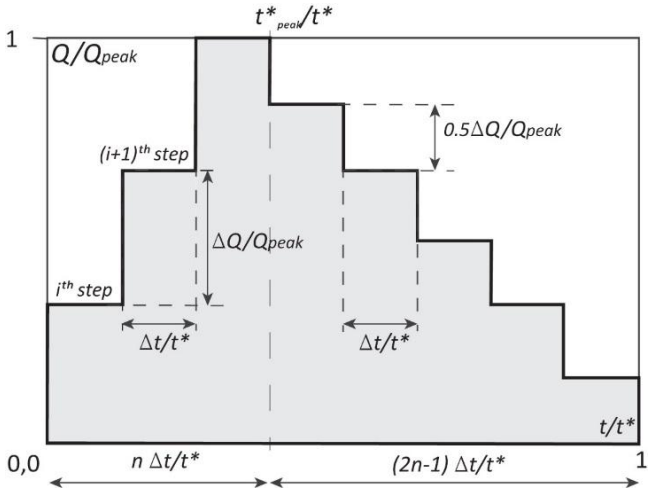

Fig. 3. Test hydrograph showing n = 3 steps in the rising limb.

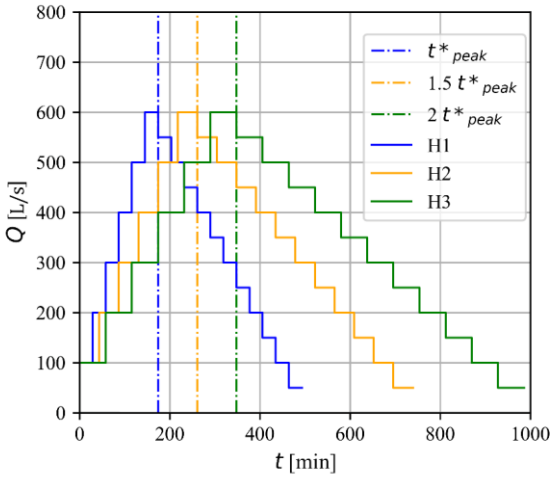

Fig. 4. Select stepped hydrographs with n = 6, Q_{peak} = 600 l/s and m = 1, 1.5 and 2 represented as H1, H2 and H3.

Table 2. Test scenarios and results.

Test	Test name ($Q_{peak}\_n\_m$)	Q_{peak} [l/s]	n	m	ΔQ [l/s]	Δt [min]	t^* [hrs]	Z_{max} [m]	Z_{eq} [m]	X_{max} [m]	L_{max} [m]
1	Steady_150	150	-	-	-	(steady)	7.5	0.280	0.280	0.400	1.070
2	Steady_300	300	-	-	-	(steady)	17.5	0.560	0.560	0.520	1.810
3	Steady_600	600	-	-	-	(steady)	19.5	1.010	1.010	1.000	3.190
4	300_3_1	300	3	1	100	37.0	4.9	0.452	0.415	0.355	1.455
5	300_6_1	300	6	1	50	18.5	5.2	0.438	0.415	0.455	1.355
6	300_9_1	300	9	1	33.3	12.3	5.3	0.453	0.437	0.455	1.455
7	600_3_1	600	3	1	200	58.0	7.7	0.694	0.676	0.705	2.155
8	600_6_1	600	6	1	100	29.0	8.2	0.710	0.676	0.805	2.155
9	600_9_1	600	9	1	66.7	19.3	8.4	0.710	0.670	0.705	2.055
10	300_6_1.5	300	6	1.5	33.3	27.8	7.9	0.460	0.435	0.450	1.305
11	300_6_2	300	6	2	33.3	37.0	10.9	0.473	0.447	0.505	1.505
12	600_6_1.5	600	6	1.5	66.7	43.5	12.3	0.756	0.705	0.755	2.205
13	600_6_2	600	6	2	66.7	58.0	16.4	0.770	0.723	0.805	2.255

3 RESULTS

3.1 Scour evolution under steady flows

Vertical and inclined jets from the inlet and outlet keys of the PKW impinged on the alluvial bed and began the formation of a scour hole. For fixed discharge or steady-state flow conditions, scour hole evolution increased rapidly in both vertical and longitudinal directions, following an asymptotic path and eventually reaching equilibrium. Although this process is specific to the PKW, Type A PKW (Lantz et al., 2022) and TPKW (Chooplou et al., 2022), similarities with other hydraulic structures were observed, including bed sills (Ben Meftah and Mossa, 2006) and vertical drop (Dey and Raikar, 2007) (see Fig 5), which included three different phases of scour development per Ben Meftah and Mossa (2006) (Fig. 5): 1) the initial phase, where the scour rapidly increases reaching the 65% of the equilibrium value; 2) the transition phase where the scour gradually increases to 90% of the total scour; and 3) the equilibrium phase, when the scour depth increases by an additional ~10%, while the kinetics of the process significantly decreases, asymptotically approaching the equilibrium value. However, it is worth remarking that recent studies by Di Nardi et al. (2023) demonstrated that other classifications including those by Zanke (1978), Ben Meftah and Mossa (2006), Dey and Sarkar (2006) and Lu et al. (2013) are basically consistent with that by Bombardelli et al. (2018) (see Sections 3.2 and 3.3. for details). Namely, two main phases can be distinguished, i.e., the developing phase (corresponding to the mentioned initial phase and part of the transition phase) and the developed phase, characterized by a proportional expansion of the scoured area up to asymptotic equilibrium configuration. According to Bombardelli et al. (2018), the transition time between these two phases depends on the impingement angle of the jet on the downstream water surface.

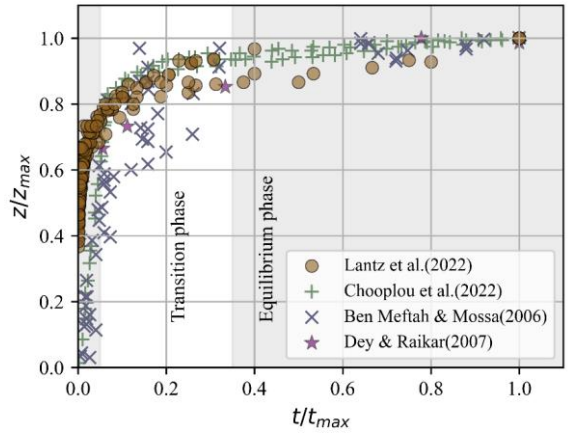

Fig. 5. Kinetics of scour evolution for different hydraulic structures, including Type A PKW, TPKW bed sills, and vertical drop structures.

3.2 Scour evolution under unsteady flows

The kinetics of scour evolution exhibits similarities to those observed under steady conditions, although some peculiar features are present. During each increasing step (characterized by a constant flow discharge), the scour velocity is a monotonic decreasing function of time (as expected local velocities decrease with local scour as flow area is increasing), with a rapid initial phase followed by a gradual reduction in the rate of scour. However, under unsteady flows, the scour kinetics also depend on the inflow conditions and simulated hydrograph. More specifically, a surge in scour was observed with each spike of inflow until the peak discharge. Conversely, an overall scour morphology stabilization was observed during the falling limb, with some exception during the first decreasing steps due to the shift of the hydraulic jump in the stilling basin caused by the reduction of the upstream momentum flux originating from the structure. In other words, during falling limb of the hydrograph, as flow discharge decreases, shear stresses applied to the alluvium cease to exceed the critical counterpart, resulting in minor settling and reorganization of the bed particles (Z_{eq} in Table 2). As an example, in Fig. 6, we show the comparison of the non-dimensional scour evolution pertaining to both reference tests and selected unsteady tests conducted for Q_{peak} = 600 l/s and 300 l/s and different values of n and m.

In the tested range of parameters, we observed a reduction in the scour hole under the unsteady flow case, compared to its steady counterpart. An average scour depth of approximately 72% of the reference equilibrium value (steady case) was achieved with the unsteady flow simulations (Table 2, Fig. 6), plotted against the non-dimensional time T that is a function of t, L_c, gravity (g), the 90th percentile grain diameter d_{90}, density of the sediment and water (ρ_s and ρ respectively) (Bombardelli et al., 2018). Fig. 6 shows the ratio of scour to steady flow case, which is less than unity for the duration of unsteady flow test. It also highlights that for the same timestep; unsteady flow scour is around 90% of the steady state counterpart. Likewise, location of maximum scour depth, X_{max} and length of scour hole, L_{max} attained during the unsteady flow simulation also compares to ~70% of the location and length of scour during the steady flow simulation. This highlights that scour relationships valid for steady state flow case may slightly overestimate the maximum scour depth.

Very importantly, it can be observed that the maximum scour procured with different hydrograph configurations (n and Δt) are within 10% (Table 2). This shows that the minimum duration to achieve the consistent scour features acquired using the time to peak (t^*_{peak}) calculated with Eq. (1) valid for low head structures can be used for PKW structures with agreeable performance. Please also note that for the hydrograph configurations, some marginal additional scour occurred on the falling limb after Q_{peak}, highlighting the value of the duration of the flow at Q_{peak} and the shape of the hydrograph in the context of scour phase of substrate.

Scour morphology is generally three-dimensional with deeper scour formations occurring downstream of the inclined jets where flows converge in the outlet ramp. Initially, the scour hole has an elongated shape and is confined both downstream and in the sides by a sediment deposition (Fig. 7a). The impingement angle of jet on the water surface decreases with discharge, resulting in the downstream shift of the location of the maximum scour depth. Due to the structural restriction in the upstream area, the scour hole evolves into a spoon shape with a downstream ridge which gradually gets eroded, thus enhancing further scour development (Figs. 7b-e). However, the complex geometry of PKW reflects into a complex jet dynamic, with the inclination of the impinging jets ranging between 30° (at the outlet section) and 80° (at the inlet section) for low flow case. Therefore, in the following we consider the average angle of impingement of the jet, i.e., α = 55°. It is worth remarking that, during falling limb, the scour hole did not significantly alter its morphology, i.e., the location of the maximum scour depth does not shift (Figs. 7g-h).

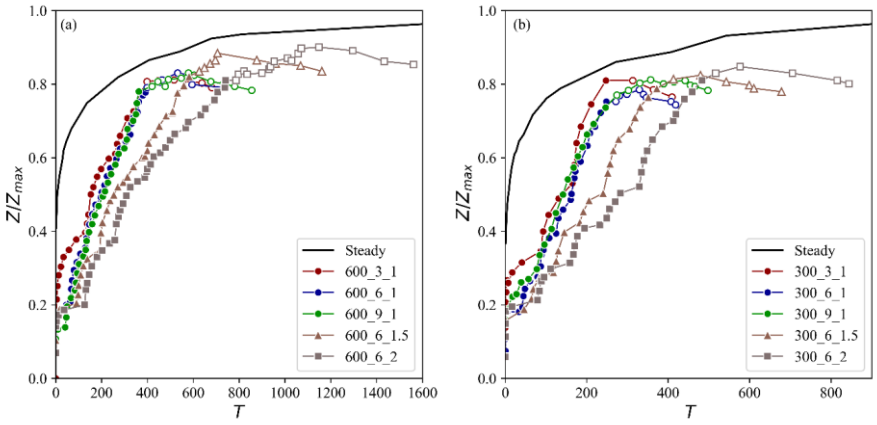

Fig. 6. Z/Z_{max} as function of non-dimensional time T for tests conducted under both steady and unsteady conditions with Q_{peak} equal to a) 600 l/s and b) 300 l/s. The solid color represents the rising limb and hollow symbols represent the falling limb. (Z_{max} here is adopted from steady flow case).

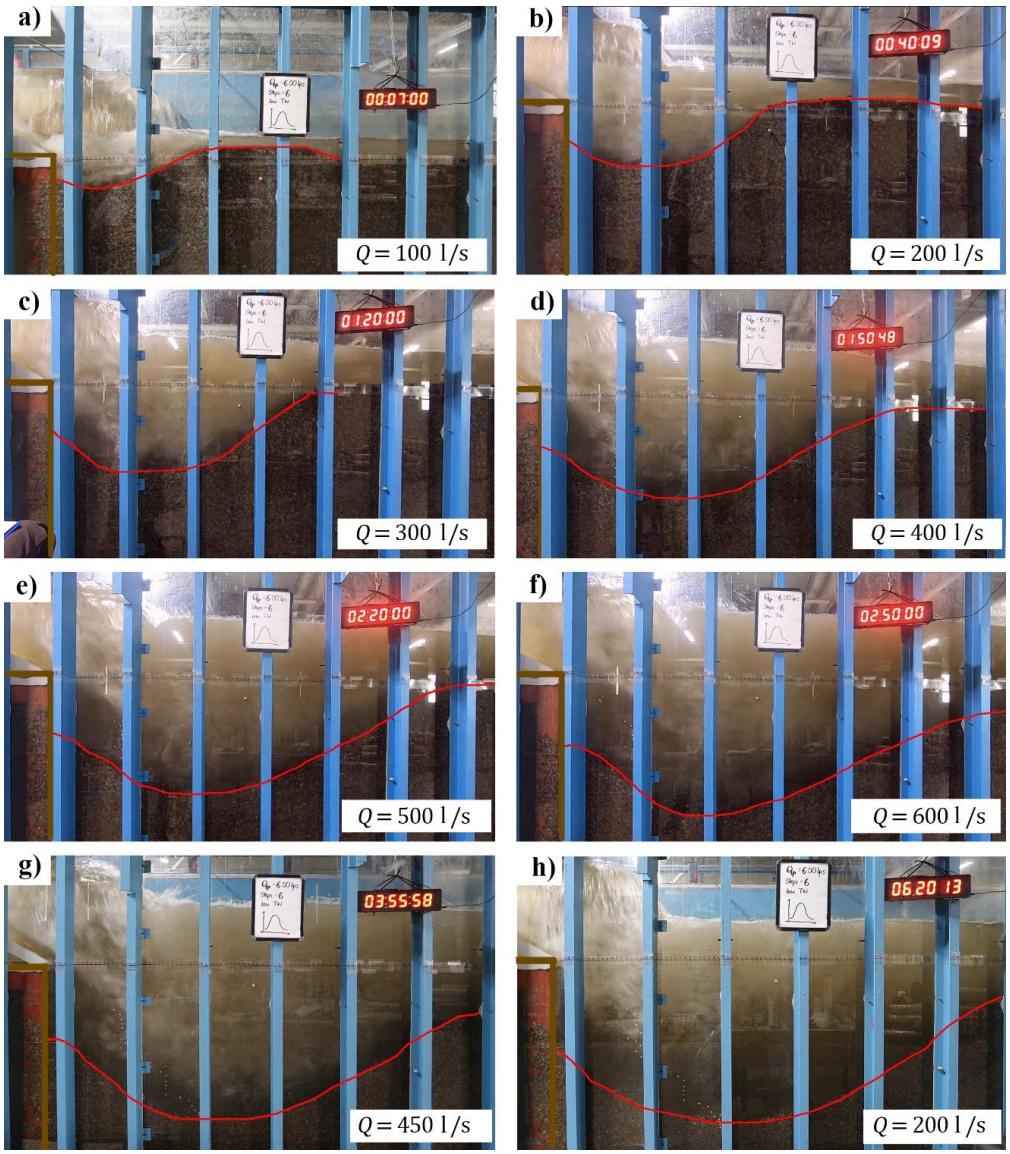

Fig. 7. Scour evolution at different steps for an unsteady test with Q_{peak} = 600 l/s, n = 6. Pictures (a) to (f) pertain to the rising limb, whereas (g) and (h) show two stages in the falling limb. The clock time shows the time from the start of the test and Q represents the value of the discharge in each stage.

3.2.1 Scour similitude

In this study, the similitude of the scour profiles was assessed by analyzing the development of the scour geometry as a function of the non-dimensional time *T*. Following Di Nardi et al. (2022) and (2023), this comparison was performed for both steady and unsteady cases to verify if the basic assumptions of the PTT model also apply to PKWs. More specifically, according to Bombardelli et al. (2018) and Di Nardi et al. (2022), a scour profile similitude with a homothetic (i.e., a proportional) expansion of the scour hole should occur during the developed phase.

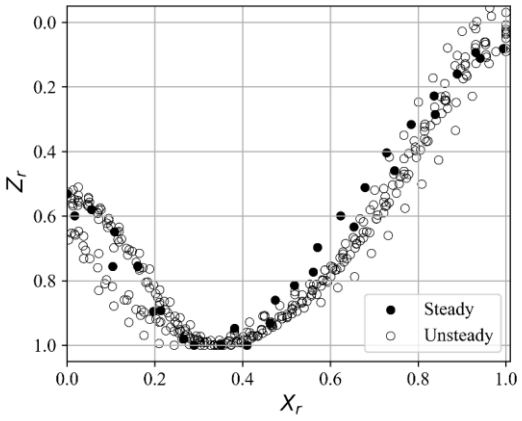

Fig. 8. Longitudinal scour profiles at equilibrium for both steady and unsteady flow cases.

Therefore, we conducted our analysis in two steps. First, the non-dimensional equilibrium scour profiles pertaining to all tests were compared. Fig. 8 shows such comparison by contrasting the non-dimensional vertical coordinate (Z_r = z/Z_{max}) against the non-dimensional longitudinal coordinate (X_r = x/L_{max}), with *x* and *z* representing the longitudinal and vertical coordinate and L_{max} and Z_{max} the maximum scour length and depth at the end of the test, respectively. Experimental data reveal that a substantial profile similitude also occurs for the PKWs under both steady and unsteady flow cases.

Then, the non-dimensional transition time T_T between the developing and developed phases was estimated according to Bombardelli et al. (2018):

$$\log T_T = -0.02\alpha + 3.62 \quad (2)$$

More specifically, to ascertain the occurrence of a homothetic expansion of the scour hole during the developed phase, in Fig. 9 we contrast the values of the ratio *L*/*Z* against the respective non-dimensional times *T*, along with the plot of Eq. (2), with α = 55°.

It can be observed that for the unsteady cases, *L*/*Z* is affected by ΔQ and ΔT and can result in some fluctuations particularly for T < 200. However, *L*/*Z* generally decreases with *T* during the developing phase (i.e., for $T < T_T$), tending to a constant value in the developed phase (i.e., for $T > T_T$) that is either relatively aligned with the steady state tests or slightly greater, such as for ΔQ = 50 l/s (trending towards *L*/*Z* = 4.0). This constant value occurrence indicates that a homothetic expansion of the scour hole takes place and is in full agreement with results obtained by Di Nardi et al. (2022) for sub-vertical plunging jets. Overall, general behavior in scour mechanisms is confirmed, regardless of the hydraulic structure configuration. However, it is worth remarking that during the developing phase, *L*/*Z* is also affected by ΔQ and ΔT, because of the modification induced by the shift of the hydraulic jump in the downstream alluvial bed resulting in a variation of local velocities, shear on the bed, and sediment dynamics within the scour hole.

3.3 Application of Phenomenological Theory of Turbulence (PTT model)

Bombardelli et al. (2018) developed the following Eqs. (3) and (4) to estimate the parameter $R_{eq} = Z_{max} + h_d$ where R_{eq} is the value of *R* at equilibrium and the temporal evolution of the maximum scour depth Z_{max} for the 3D case:

$$R_{eq} = k_1 \left(\frac{\rho}{\rho_s - \rho}\right)^{3/5} (Qh)^{2/5} {d_{50}}^{-2/5} g^{-1/5} \quad (3)$$

$$\frac{dZ}{dt} = k_7 \sqrt{\frac{(\rho_s - \rho) g d^5}{\rho {h_d}^2}} \frac{1}{Z} \left[\left(\frac{R_{eq}}{R}\right)^{5/3} - 1\right]^{m_2} \quad (4)$$

with *h* indicating the falling height, total scour depth $R = Z + h_d$, with *Z* being the scour depth and h_d being the tail water depth at time *t*, and k_1 = 0.5, k_7 = 80 and m_2 = 1.5 are constants. It is worth remarking that the values of constants k_1 and k_7 were derived for vertical and sub-vertical plunging jets, whereas the constant m_2 is valid for non-cohesive sediment (Yalin, 1977; Julien, 2018). Successively, Di Nardi et al. (2023) tested different values of the constant k_7, showing that lower values (e.g., 0.3) may improve the overall predicting capability of Eq. (4) for several grade control structures.

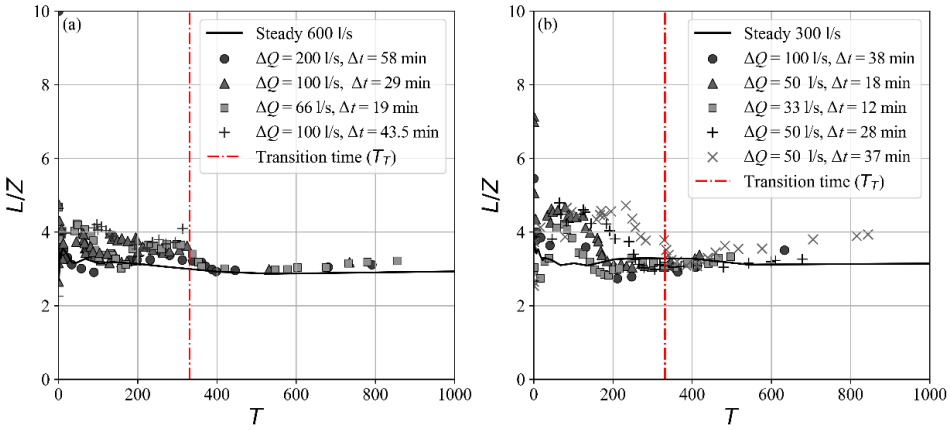

Fig. 9. Evolution of the ratio *L*/*Z* for selected tests with Q_{peak} as a) 600 l/s b) 300 l/s under both steady and unsteady flow conditions.

According to Di Nardi et al. (2022) and (2023), the ordinary differential equation presented in Eq. (4) can also be successfully applied to the unsteady cases as well. For each *i*-step, the numerical solution of Eq. (4) can be obtained by assuming $R_{eq} = R_i = Z_i + h_{di}$, with Z_i and h_{di} representing the maximum scour depth and the water level of the *i*-step of the increasing phase of the hydrograph (i.e., for $i \leq n$), characterized by a constant discharge Q_i and a duration equal to Δt. As for the initial conditions (subscript *in*), for the first step, we set t_{in} as the time at which the we took the first scour depth measurement Z_{in}, i.e., generally $t_{in} \approx$ 5-10 s; for the (*i*+1)-step, $t_{in} = i\Delta t$ and $Z_{in} = Z_i$. Likewise, for the parameter R_i (i.e., R_{eq} in Eq. 4) we consider three different methods: R_i is set equal to 1) the experimental value; R_i is estimated using 2) Eq. (3) and 3) the empirical equation (5) proposed by Justrich et al. (2016):

$$Z_{max} = 0.42\, d_{50} \left(\frac{h_c}{d_{50}}\right)^{1.7} \left(\frac{\Delta H}{h_d}\right)^{0.3} \quad (5)$$

with h_c indicating the critical depth. Details for methods 2) and 3) are provided in section 3.3.2.

This approach allows us to first evaluate the predicting capability of Eqs. (3) and (4) by analyzing their sensitivity to the constants k_1 and k_7 under steady case, and then to extend the analysis to the unsteady flow conditions.

3.3.1 Calibration of values of constants k_1 and k_7 for PKWs

For the steady case, results from selected experiments by Lantz et al. (2022) were employed to analyze the sensitivity of Eq. (3) to the constant k_1. Namely, we tested different values of k_1 to assess the predicting capability of Eq. (3) of the equilibrium scour depth for PKWs. The least error (RMSE = 0.194) is obtained with $k_1 = 0.51$ (Fig. 10), that is basically the same value proposed by Bombardelli et al. (2018) for scour caused by inclined jets (i.e., $k_1 = 0.5$).

A similar analysis was conducted for the coefficient k_7. To this end, scour evolution data pertaining to steady tests conducted by Lantz et.al. (2022) with discharges Q = 600 l/s, 300 l/s and 150 l/s were employed. Namely, non-dimensional scour depth values Z/Z_{max} were plotted as a function of the non-dimensional time T along with the numerical solutions of Eq. (4) pertaining to different values of k_7, ranging from 0.3 to 5. It is worth remarking that the scour rate dZ/dt is a monotoning increasing function of k_7. In other words, the constant k_7 reflects the kinetics of the scour mechanism, all other parameters being constant. For jet scour Bombardelli et al. (2018) proposed k_7 = 80, whereas Di Nardi et al. (2023) observed lower rate of scour evolution for low head structure with k_7 = 0.3 being more significant in capturing the scour evolution. This is due to the fact that the scour dynamics characterizing plunging jets is slightly different from that occurring downstream of sills and grade-control structures. As for the PKWs, Eq. (4) notably captures the scour depth evolution observed during the experiment (Fig. 11). Apparently, the kinetics of the scour process slightly depends on the jet geometry but more so on flow discharge and resulting forces imparted on the substrate. This jet mechanic observation may be due to the very complex and peculiar flow dynamics of the PKWs, where a combination of jet flows with different impinging angles on the water surface take place.

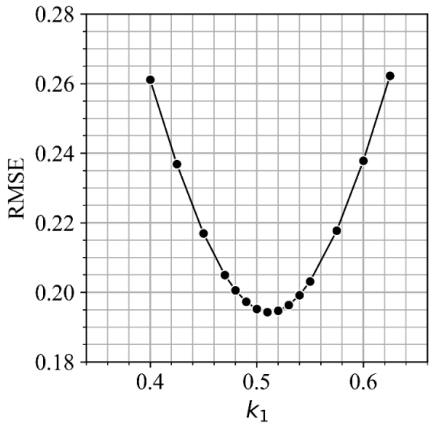

Fig. 10. Root mean square error for different values of k_1.

The sensitivity of k_7 is also checked for the unsteady flow case, as shown in Fig. 12, where scour data pertaining to selected tests are plotted against T along with the numerical solution of Eq. (4), obtained adopting the procedure described in Section 3.3 with R_i equal to the experimental value. Overall, the scour kinetics appear to be consistent with that of the steady counterpart. Namely, for higher k_7 values we can observe an increase in the scour rate in each *i*-step. It is worth remarking that for unsteady cases, steep rise in scour evolution occurs with each increment of discharge value, which is harder to capture using smaller values of k_7. Therefore, based on experimental evidence for both steady and unsteady case, in order to provide a general relationship valid for all the cases, a value of k_7 = 5 is considered to be representative of the kinetics of the scour process for PKWs, resulting in a deviation between measured and predicted values of scour depth that is common for scour related-problems and in line with other approaches.

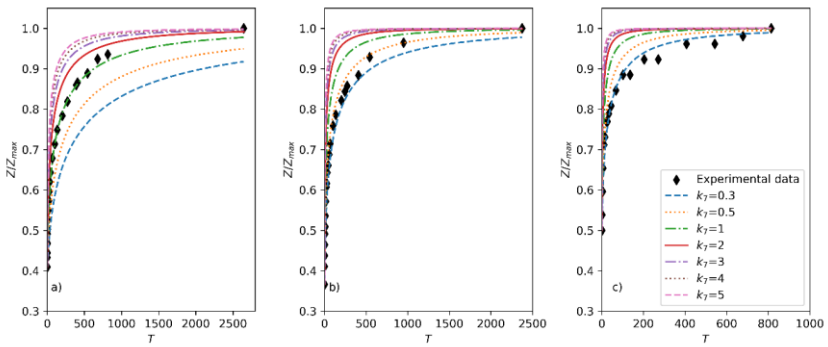

Fig. 11. Sensitivity of the constant *k*7 value for temporal scour evolution using steady state scour data from Lantz et. al. (2022) for Q a) 600 l/s, b) 300 l/s and c) 150 l/s.

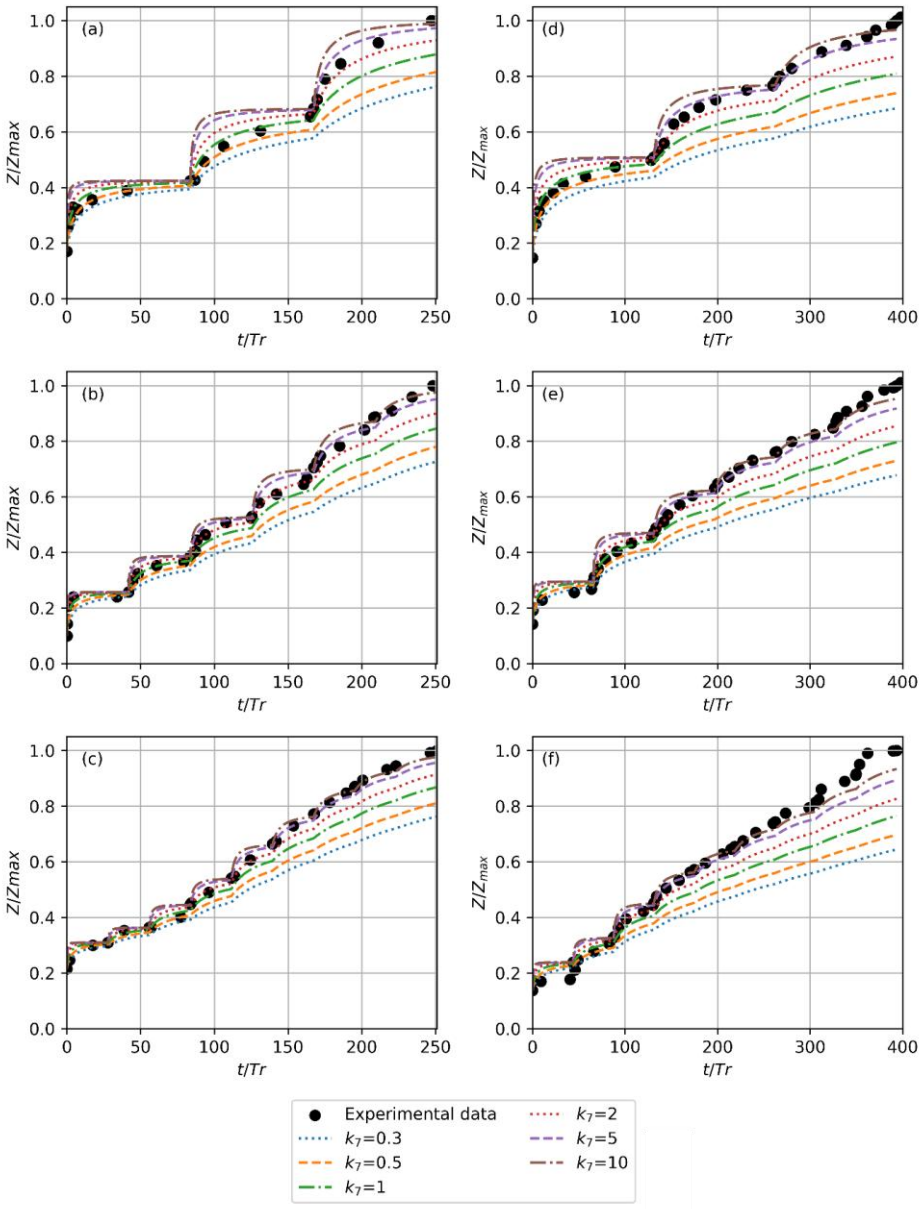

Fig. 12. Sensitivity of k_7 value for selected unsteady tests with Q_{peak} = 300 l/s and a) n = 3, b) n = 6 and c) n = 9 and with Q_{peak} = 600 l/s and d) n = 3, e) n = 6 and f) n = 9.

3.3.2 Validation of the PTT evolution model for PKWs under unsteady flow conditions

Toe scour prediction is compared using three different methods to set the value of R_i pertaining to each i-step in Eq. (4). First, to assess that the PTT model is able to correctly interpret the evolution of the scour for the entire data set, we assume R_i equal to the experimental value, given by the sum of the maximum measured scour depth Z_i and the tail water depth h_{di} for each discharge steps. In Fig. 13, we show the evolution of the relative scour depth Z/Z_{max} as function of the non-dimensional time T for m = 1. Overall, the agreement of experimental data with numerical solution of Eq. (4) (red dashed curves) appears extremely good, meaning that the PTT model is able to reproduce the physics of the scour mechanism with high accuracy.

However, in order to provide a predictive methodology that can be easily applicable by practitioners, we consider estimating R_i in two different ways, i.e., by alternatively using Eqs. (3) and (5). As for the first option, we observe that the maximum scour depth at the end of each i-step increases almost linearly with i up to reach the maximum value Z_{max} for $i = n$. In other words, we can reasonably assume that, at each i-step, the increment of the scour depth is equal to Z_{max}/n. Consequently, for the first step, we consider $Z_i = Z_1 = Z_{max}/n$; then, the maximum scour depth pertaining to the step i+1 is set equal to $Z_{i+1} = Z_i + Z_{max}/n$, resulting in $Z_i = Z_n = Z_{max}$ for the last step (i.e., for $i = n$). The value of the maximum scour depth Z_{max} is estimated using Eq. (3) with k_1 = 0.5, from which we derive R_{eq} and, consequently, $Z_{max} = R_{eq} - h_d$. (Note that Z_{max} is the maximum scour depth relative to the corresponding reference steady flow condition with $Q = Q_{peak}$.) Under this assumption, we can now numerically solve Eq. (4). Alternatively, Z_i pertaining to each i-step can be estimated by using Eq. (5), with the critical depth h_c, the energy

head ΔH and the tailwater level h_d equal to the corresponding values h_{ci}, ΔH_i and h_{di} pertaining to the discharge Q_i of the i-step. Like in the previous case, by knowing the values of Z_i, we can apply Eq. (4) to all the i-steps. It is worth remarking that in both the cases, based on the findings of the previous section, k_7 is set equal to 5.

Numerical solutions obtained via the mentioned methods are also plotted in Fig. 13 and compared with those obtained adopting measured values of R_i in Eq. (4). (Note that in Fig. 13 the measured value of Z_{max} is used to make the scour depth non dimensional for all the numerical solutions.) Overall, we can observe that experimental data are always overpredicted when using empirical Eq. (5) to estimate Z_i (green dashed curves). Conversely, mixed results are obtained with the theoretical Eq. (3) applied following the methodology illustrated above (blue dashed curves). This behavior can be explained considering that Eq. (5) systematically overestimates the equilibrium scour depths pertaining to the i-step. This is because Eq. (5) was developed under steady flow conditions at equilibrium. In contrast, in the tested range of parameters, the duration of each step of the hydrograph only allowed the scour to reach a quasi-equilibrium configuration for hydraulic conditions relative to each i-step. Similar results can be observed for different durations of hydrograph, i.e., for m = 1.5 and 2 (Fig. 14).

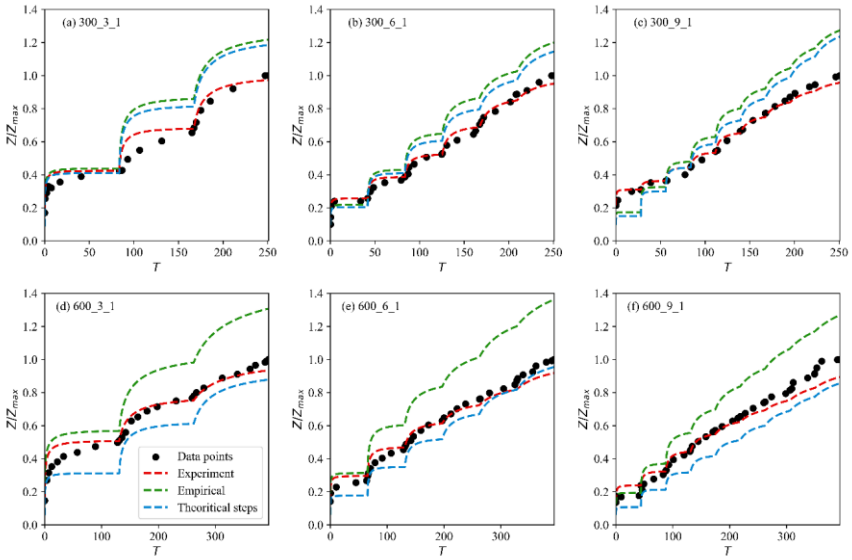

Fig. 13. Scour depth evolution for tests with t^*_{peak} for a) 300 l/s with 3 steps, b) 300 l/s with 6 steps, c) 300 l/s with 9 steps, d) 600 l/s with 3 steps, e) 600 l/s with 6 steps and f) 600 l/s with 9 steps, comparing experiment data points with results using empirical, theoretical and experiment data. Z_{max} is taken as the maximum measured scour depth for comparison.

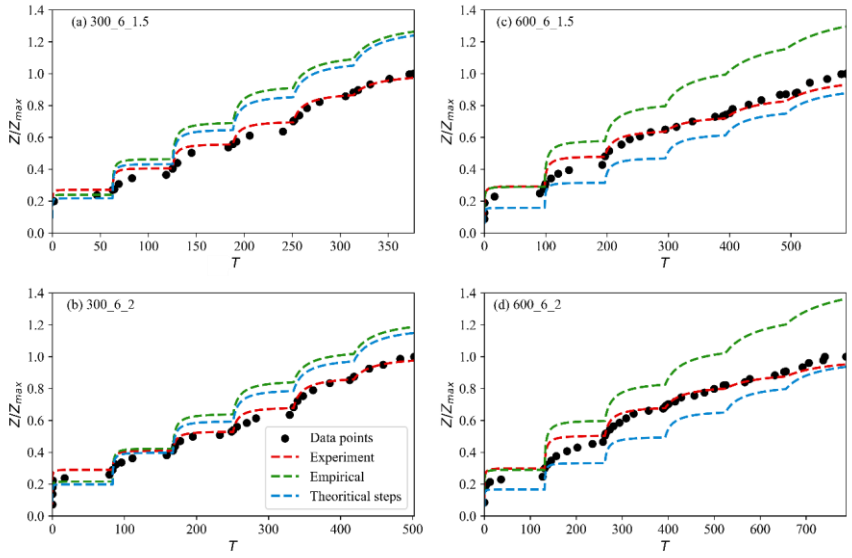

Fig. 14. Scour depth evolution for tests with 6 steps and m = 1.5 and 2 for a) 300 l/s with m = 1.5, b) 300 l/s with m = 2, c) 600 l/s with m = 1.5 and d) 600 l/s with m = 2 comparing experiment data points with results using empirical, theoretical and experimental data. Z_{max} is taken as the maximum measured scour depth for comparison.

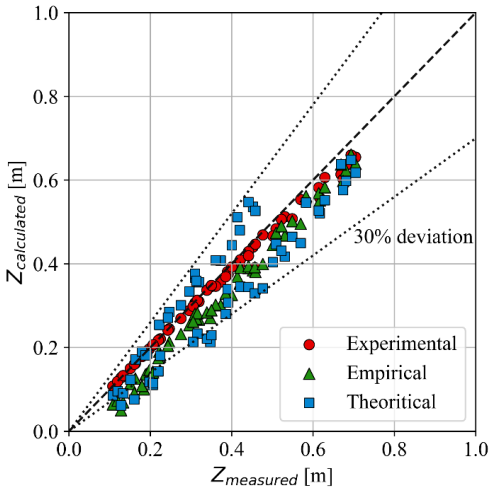

Fig. 15. Comparison between measured and predicted values of the scour depth during the evolution using the temporal evolution with values from experimental dataset, corrected empirical, and PTT theoretical formula.

Results of comparison between measured and calculated values of the scour depth evolution pertaining to all tests are reported in Fig. 15. Initially, empirical values via Eq. 5 (developed for the steady state case) were approximately 10-30% greater than the unsteady experimental values Z, but by applying an unsteady calibration coefficient $\zeta = 0.7$, $Z_{calculated}$ via Eq. 5 are in closer agreement. However, the authors recommend the theoretical PTT approach as it is based upon the physics of local scour and provides reasonable accuracy. To summarize, for the theoretical model the RMSE, NSE, and R^2 values were 0.067, 0.806, and 0.972, respectively. For Eq. 5 multiplied by $\zeta = 0.7$, RMSE, NSE, and R^2 values were 0.044, 0.915, and 0.993 with less accuracies noted for $Z < 0.2$. Note that ζ is for the specific cases tested herein and could be further refined to be a function to this or an independent dataset for Eq. 5. Overall, as presented we can observe a reasonable agreement, within 30% error range.

4 CONCLUSIONS

The analysis of scour evolution under steady flow and variable flow conditions was conducted for Type A PKW structure with alluvial cohesionless bed using experimental datasets. The scour comparison showed an overall decrease in scour both vertically and longitudinally by nearly 30% during the unsteady flow case compared to its steady flow counterpart, highlighting those results using steady flow case usually provide an overestimation of scour dimensions. An effort to validate the scour evolution predicting capability of the PTT model in collaboration with the theoretical formula and the empirical formula was performed next. Particularly the scour evolution at the toe or base of the PKW was characterized to comply the requirements of the PTT model with the homothetic expansion of scour holes and the scour similitude. After assessing the scour and the validity of the PTT theory, the model prediction was checked for scour at PKW with selecting the right values for different constants by doing a sensitivity analysis. In doing so, values of constants were selected such that they provide reasonable results for all the cases with minimum errors. The multiplicative constants providing coherent results were $k_1 = 0.5$, $k_7 = 5$ and $m_2 = 1.5$.

Later on, the comparison of model prediction in combination with theoretical scour estimation and with the scour estimation using empirical formula was done against the experimental data and it was observed that the results lay within 30% of error range. The model prediction using experimental data sets showed the best agreeable results. Prediction using theoretical scour values showed both over and underprediction of scour whereas prediction using empirical equation was observed to have almost 30% over prediction. The overprediction using empirical equation reflects with overprediction of scour during steady flow case, as the formula was developed using steady flow cases.

Overall, it can be observed that the PTT model provides significant insights on predicting the temporal scour evolution and use of PTT model with theoretical and empirical equation can be of practical significance showing accurate estimates of the scour evolution without the hassle of performing experimental tests.

Acknowledgement: This research was conducted at the Utah Water Research Laboratory; the authors express their gratitude for the support provided to complete this research.

Open access: All experimental scour data and the temporal evolution analysis code pertaining to this study are available at http://www.hydroshare.org/resource/74df51f215894747818db8d313916460 (see Panthi 2025b).

NOTATION

The following symbols are used in this study:

a, b, c, d, k	empirical constants using experimental data
α	angle of jet
B	total width of the piano key weir (B_i+B_b+B_o)
B_b	base of the piano key weir
B_i	inlet key length
B_o	outlet key width
d_{50}	median grain size diameter
d_{90}	90th percentile grain size diameter
g	gravitational constant
G	specific density
h_c	critical flow depth
h_d	tail water flow depth on initial bed
H_u	upstream reservoir head
ΔH	energy head
i	incremental step
k_1	multiplicative constant
k_7	multiplicative constant
L	length of toe scour
L_c	length of the piano key weir crest
L_{max}	length of the maximum toe scour
N	number of piano key weir cycles or keys
n	total number of steps in the rising limb
m	t^*_{peak} multiplier
m_2	constant
P	height of the piano key weir

P_d	depth of the piano key weir footing
Q	discharge
Q_{peak}	peak discharge
R	scour depth ($Z+h_d$)
R_{eq}	scour depth at equilibrium conditions
RMSE	root mean square error
ρ	density of water
ρ_s	density of sediment particle
σ	coefficient of gradation
T	non-dimensional time $\left(T = \frac{t}{L_c}\left[g d_{90} \frac{(\rho_s-\rho)}{\rho}\right]^{0.5}\right)$
t	time from the onset of the test
t_{peak}	time to peak
t^*	total duration of the hydrograph
T^*_{peak}	nondimensional time to peak taken as 3200
t^*_{peak}	duration until the peak flow
Δt	duration of each step
t_s	thickness of the piano key weir wall
T_T	non-dimensional transition time ($log\ T_T$ = -0.02α+3.62)
W	width of flume
W_i	width of the inlet key
W_o	width of the outlet key
W_u	width of a unit PKW cycle
X	location of scour in streamwise direction x
x	streamwise coordinate
X_{max}	location of the maximum toe scour
X_r	nondimensional streamise or longitudinal coordinate
Z	toe scour depth
z	vertical coordinate with down as positive
ΔZ	bed level relative to weir toe
Z_{eq}	equilibrium toe scour value
Z_{max}	maximum toe scour value
Z_r	nondimensional vertical coordinate
ζ	unsteady scour calibration coefficient for Eq. 5
Subscripts	
c	critical
in	initial
max	maximum value
eq	equilibrium value
i	inlet or at an instant or step i
N	at final step
o	outlet
$peak$	peak value
r	nondimensional parameter
T	Transition value
u	Piano key weir unit

REFERENCES

Anderson, R., Tullis, B., 2012. Piano key weir: Reservoir versus channel application. Journal of Irrigation and Drainage Engineering, 138(8), 773–776. https://doi.org/10.1061/(ASCE)IR.1943-4774.0000464

Annandale, G. W. 1995., Erodibility. J. Hydraul. Res., 33 (4): 471–494. IAHR Website. https://doi.org/10.1080/00221689509498656.

Ben Meftah, M., Mossa, M., 2006. Scour holes downstream of bed sills in low-gradient channels. Journal of Hydraulic Research, 44(4), 497–509. https://doi.org/10.1080/00221686.2006.9521701

Bermúdez, M., Farfán, J. F., Willems, P., Cea, L., 2021. Assessing the Effects of Climate Change on Compound Flooding in Coastal River Areas. Water Resources Research, 57(10), e2020WR029321. https://doi.org/10.1029/2020WR029321

Bombardelli, F. A., Gioia, G., 2006. Scouring of granular beds by jet-driven axisymmetric turbulent cauldrons. Physics of Fluids, 18(8), 088101. https://doi.org/10.1063/1.2335887

Bombardelli, F. A., Palermo, M., Pagliara, S., 2018. Temporal evolution of jet induced scour depth in cohesionless granular beds and the phenomenological theory of turbulence. Physics of Fluids, 30(8), 085109. https://doi.org/10.1063/1.5041800

Bormann, N. E., Julien, P.Y., 1991. Scour Downstream of Grade-Control Structures. Journal of Hydraulic Engineering, 117(5), 579–594. https://doi.org/10.1061/(ASCE)0733-9429(1991)117:5(579)

Brunner, M. I., Viviroli, D., Sikorska, A. E., Vannier, O., Favre, A.-C., Seibert, J., 2017. Flood type specific construction of synthetic design hydrographs. Water Resources Research, 53(2), 1390–1406. https://doi.org/10.1002/2016WR019535

Burns, S. E., Bhatia, S. K., Avila, C. M. C., Hunt, B. E. (Eds.)., 2010. Scour and Erosion. In In Proceedings of the Fifth International Conference on. San Francisco, California, United States: ASCE Publications. https://doi.org/10.1061/9780784411476

Cea, L., Costabile, P., 2022. Flood Risk in Urban Areas: Modelling, Management and Adaptation to Climate Change. A Review. Hydrology, 9(3), 50. https://doi.org/10.3390/hydrology9030050

Chanson, H., Felder, S., 2017. Hydraulics of Selected Hydraulic Structures. In Open Channel Hydraulics, River Hydraulic Structures and Fluvial Geomorphology. CRC Press.

Chooplou, C. A., Kazerooni, S., Ghodsian, M., Vaghefi, M., 2022. Experimental study of scouring downstream of type-A piano key weirs. Arabian Journal of Geosciences, 15(23), 1702. https://doi.org/10.1007/s12517-022-11001-9

Copeland, R. R., McComes, D. N., Thorne, C. R., Soar, P. J., Megh M., J., and Fripp, J.B., 2001. Hydraulic Design of Stream Restoration Projects (p. 172). US Army Corps of Engineers. Retrieved from https://apps.dtic.mil/sti/citations/ADA400662

Crookston, B., Erpicum, S., Tullis, B., Laugier, F., 2019. Hydraulics of labyrinth and piano key weirs: 100 years of prototype structures, advancements, and future research needs. Journal of Hydraulic Engineering, 145(12), 02519004. https://doi.org/10.1061/(ASCE)HY.1943-7900.0001646

Crookston, B. M., Anderson, R. M., Tullis, B.P., 2018. Free-flow discharge estimation method for Piano Key weir geometries. Journal of Hydro-Environment Research, 19, 160–167. https://doi.org/10.1016/j.jher.2017.10.003

D'Agostino, V., Ferro, V., 2004. Scour on Alluvial Bed Downstream of Grade-Control Structures. Journal of Hydraulic Engineering, 130(1), 24–37. https://doi.org/10.1061/(ASCE)0733-9429(2004)130:1(24)

Dey, S., Raikar, R.V., 2007. Scour below a High Vertical Drop. Journal of Hydraulic Engineering, 133(5), 564–568. https://doi.org/10.1061/(ASCE)0733-9429(2007)133:5(564)

Dey, S., Sarkar, A., 2006. Scour Downstream of an Apron Due to Submerged Horizontal Jets. Journal of Hydraulic Engineering, 132(3), 246–257. https://doi.org/10.1061/(ASCE)0733-9429(2006)132:3(246)

Di Nardi, J., Palermo, M., Bombardelli, F. A., Pagliara, S., 2021. The phenomenological theory of turbulence and the scour evolution downstream of grade-control structures under steady discharges. Water, 13(17), 2359.

Di Nardi, J., Palermo, M., Bombardelli, F. A., Pagliara, S., 2022. First Principles-Based Approach for 3D Scour Processes Under Variable Jet Discharge. Water Resources Research, 58(11), e2021WR030346. https://doi.org/10.1029/2021WR030346

Di Nardi, J., Palermo, M., Bombardelli, F. A., Pagliara, S., 2023. Scour evolution downstream of grade-control structures under unsteady flows: A theoretical analysis. Journal of Hydro-Environment Research, 48, 1–14. https://doi.org/10.1016/j.jher.2023.04.001

Erpicum, S., Lempérière, F., Ouamane, A., Khanh, M. H. T., Laugier, F., Tullis, B., Crookston, B., 2020. From labyrinth to piano key weirs: the story. International Association for Hydraulic Research, Hydrolink(4–2020). Retrieved from https://static.iahr.org/library/HydroLink/HL2020_4/HL_2020_4_piano_key_weirs.pdf

Ettema, R., Yoon, B., Nakato, T., Muste, M., 2004. A review of scour conditions and scour-estimation difficulties for bridge abutments. KSCE Journal of Civil Engineering, 8(6), 643–650. https://doi.org/10.1007/BF02823555

Ettema, R., Constantinescu, G., Melville, B., 2011. Evaluation of bridge scour research: Pier scour processes and predictions.

Gioia, G., Bombardelli, F.A., 2005. Localized Turbulent Flows on Scouring Granular Beds. Physical Review Letters, 95(1), 014501. https://doi.org/10.1103/PhysRevLett.95.014501

Guan, D., Melville, B. W., Friedrich, H., 2015. Live-Bed Scour at Submerged Weirs. Journal of Hydraulic Engineering, 141(2), 04014071. https://doi.org/10.1061/(ASCE)HY.1943-7900.0000954

Hager, W.H., Boes, R.M., 2014. Hydraulic structures: a positive outlook into the future, 52(3), 299–310. https://doi.org/doi.org/10.1080/00221686.2014.923050

Hager, W.H., Schleiss, A.J., Boes, R.M., Pfister, M., 2020. Hydraulic Engineering of Dams. London: CRC Press. https://doi.org/10.1201/9780203771433

Heller, V. 2011. Scale effects in physical hydraulic engineering models. Journal of Hydraulic Research, 49(3), 293–306. https://doi.org/10.1080/00221686.2011.578914

Hoffmans, G.J.C.M., 1997. Scour Manual. London: Routledge. https://doi.org/10.1201/9780203740132

Hoffmans, G.J.C.M., Pilarczyk, K.W., 1995. Local Scour Downstream of Hydraulic Structures. Journal of Hydraulic Engineering, 121(4), 326–340. https://doi.org/10.1061/(ASCE)0733-9429(1995)121:4(326)

Hoffmans, G.J.C.M., 2009. Closure problem to jet scour. Journal of Hydraulic Research, 47(1), 100-109. https://doi/10.3826/jhr.2009.3179

Hoffmans, G.J.C.M., Verheij, H.J., 1997, Scour Manual. AA Balkema, https://doi.org/10.1201/9780203740132

Julien, P.Y., 2018. River Mechanics. Cambridge University Press.

Jüstrich, S., Pfister, M., Schleiss, A.J., 2016. Mobile riverbed scour downstream of a piano key weir. Journal of Hydraulic Engineering, 142(11), 04016043. https://doi.org/10.1061/(ASCE)HY.1943-7900.0001189

Knight, D.W., 2013. River hydraulics – a view from midstream, 51, 2–18. https://doi.org/doi.org/10.1080/00221686.2012.749431

Kumar, B., Ahmad, Z., 2022. Scour Downstream of a Piano Key Weir with and without a Solid Apron. Journal of Irrigation and Drainage Engineering, 148(1), 04021066. https://doi.org/10.1061/(ASCE)IR.1943-4774.0001647

Lança, R. 2013. Clear-water scour at single piers and pile groups.

Lantz, W., Crookston, B.M., Palermo, M., 2022. Evolution of local scour downstream of Type A PK weir in non-cohesive sediments. Journal of Hydrology and Hydromechanics, 70(1), 103–113. https://doi.org/10.2478/johh-2021-0035

Leite Ribeiro, M., Bieri, M., Boillat, J.-L., Schleiss, A., Singhal, G., Sharma, N., 2012. Discharge capacity of piano key weirs. Journal of Hydraulic Engineering, 138(2), 199–203.

Lempérière, F., Ouamane, A., 2003. The Piano Keys weir: a new cost-effective solution for spillways. International Journal on Hydropower and Dams, 10(5), 144–149.

Lu, J.-Y., Hong, J.-H., Chang, K.-P., Lu, T.-F., 2013. Evolution of scouring process downstream of grade-control structures under steady and unsteady flows. Hydrological Processes, 27(19), 2699–2709. https://doi.org/10.1002/hyp.9318

Machiels, O., Erpicum, S., Dewals, B. J., Archambeau, P., and Pirotton, M., 2011. Experimental observation of flow characteristics over a Piano Key Weir. Journal of Hydraulic Research, 49(3), 359–366.

Mediero, L., Jiménez-Álvarez, A., Garrote, L., 2010. Design flood hydrographs from the relationship between flood peak and volume. Hydrology and Earth System Sciences, 14(12), 2495–2505. https://doi.org/10.5194/hess-14-2495-2010

Melville, B.W., 2014. Scour at Various Hydraulic Structures: Sluice Gates, Submerged Bridges and Low Weirs. Australasian Journal of Water Resources, 18(2), 101–117. https://doi.org/10.1080/13241583.2014.11465444

Novak, P., Moffat, A.I.B., Nalluri, C., Narayanan, R., 2017. Hydraulic structures (3rd ed.). CRC Press. Retrieved from https://api.taylorfrancis.com/content/books/mono/download?identifierName=doi&identifierValue=10.1201/9781315274898&type=googlepdf

Pagliara, S., Kurdistani, S.M., 2013. Scour downstream of cross-vane structures. Journal of Hydro-Environment Research, 7(4), 236–242. https://doi.org/10.1016/j.jher.2013.02.002

Pagliara, S., Kurdistani, S.M., 2017. Flume experiments on scour downstream of wood stream restoration structures. Geomorphology, 279, 141–149. https://doi.org/10.1016/j.geomorph.2016.10.013

Pagliara, S., Palermo, M., 2008. Scour Control Downstream of Block Ramps. Journal of Hydraulic Engineering, 134(9), 1376–1382. https://doi.org/10.1061/(ASCE)0733-9429(2008)134:9(1376)

Pagliara, S., Hager, W.H., Unger, J., 2008. Temporal Evolution of Plunge Pool Scour. Journal of Hydraulic Engineering, 134(11), 1630–1638. https://doi.org/10.1061/(ASCE)0733-9429(2008)134:11(1630)

Palermo, M., Pagliara, S., 2017. Effect of unsteady flow conditions on scour features at low-head hydraulic structures. Journal of Hydro-Environment Research, 19, 168–178. https://doi.org/10.1016/j.jher.2017.04.001

Palermo, M., Crookston, B., Pagliara, S., 2020. Analysis of Equilibrium Morphologies Downstream of a PK Weir Structure. In World Environmental and Water Resources Congress 2020 (pp. 43–51). https://doi.org/10.1061/9780784482971.005

Panthi, M., 2025A. A Laboratory Study of Local Scour and Driftwood Effects on a Type A Piano Key Weir. Utah State University, Logan, UT, USA.

Panthi, M. 2025B. Unsteady flow temporal scour evolution in Type A Piano Key Weir, HydroShare, http://www.hydroshare.org/resource/74df51f215894747818db8d313916460

Phillips, C.B., Hill, K.M., Paola, C., Singer, M.B., Jerolmack, D. J., 2018. Effect of Flood Hydrograph Duration, Magnitude, and Shape on Bed Load Transport Dynamics. Geophysical Research Letters, 45(16), 8264–8271. https://doi.org/10.1029/2018GL078976

Rosgen, D.L., 2012. The Cross-Vane, W-Weir and J-Hook Vane Structures...Their Description, Design and Application for Stream Stabilization and River Restoration, 1–22. https://doi.org/10.1061/40581(2001)72

Schleiss, A.J., 2017. Better water infrastructures for a better world- The important role of water association. Retrieved from https://scholar.google.com/scholar_lookup?hl=en&volume=2017&publication_year=2017&pages=86-87&journal=Hydrolink&issue=3&author=A.+Schleiss&title=Better+water+infrastructures+for+a+better+world+%E2%80%93+The+important+role+of+water+associations

de Vriend, H.J., van Koningsveld, M., Aarninkhof, S.G.J., de Vries, M.B., Baptist, M.J., 2015. Sustainable hydraulic engineering through building with nature. Journal of Hydro-Environment Research, 9(2), 159–171. https://doi.org/10.1016/j.jher.2014.06.004

Wasko, C., Nathan, R., Stein, L., O'Shea, D., 2021. Evidence of shorter more extreme rainfalls and increased flood variability under climate change. Journal of Hydrology, 603, 126994. https://doi.org/10.1016/j.jhydrol.2021.126994

Yalin, M.S., Mehmet S., 1977. Mechanics of sediment transport. Oxford ; New York : Pergamon Press. Retrieved from http://archive.org/details/mechanicsofsedim0000yali_r2b9

Yazdi, A.M., Hoseini, S.A., Nazari, S., Amanian, N., 2020. Effects of weir geometry on scour development in the downstream of Piano Key Weirs. Water Supply, 21(1), 289–298. https://doi.org/10.2166/ws.2020.272

Zanke, U., 1978. Zusammenhänge zwischen Strömung und Sedimenttransport. Teil 1: Berechnung des Sedimenttransportes-allgemeiner Fall. Germany: EV. Retrieved from https://scholar.google.com/scholar?cluster=17136083873514126943&hl=en&oi=scholarr

.

Received 3 October 2025
Accepted 12 January 2026

Appendix 1

Table 1. Selected studies investigating toe scour downstream of a piano key weir.

Study	PKW		Discharge Features		Non-cohesive Bed Features			Research Outcomes/Findings
	Type	Features	Discharge Characteristics	Duration [min]	d_{50} [mm]	ρ_s [kg/m^3]	σ	
Jüstrich et al. (2016)	Type A PKW	*W*=0.665 m *P*=0.15 m *L/W*= 7.8	*Q*= 13-60 l/s *Q/W*= 0.018-0.0902 m^2/s *Hu/P*=0.07-0.47	90	1.6	2650	1.56	- Empirical formula characterizing toe scour features - $Z_{SM} = 0.42\ d_{50}\left(\frac{h_c}{d_{50}}\right)^{1.7}\left(\frac{\Delta H}{h_d}\right)^{0.3}$ -$X_{SM} = 1.20\ Z_{SM} + \frac{B_i}{2}$ -$x_S = 2.70\ Z_{SM} + B_i$
Yazdi et al. (2020)	PKW and TPKW (angle 6°)	*W*=0.5 m *P*=0.15 & 0.2 m *L/W*=5.1 RPKW 4.8 TPKW	*Q*= 19.5-32.3 l/s *Q/W* =0.039-0.0646 m^2/s	NA	7.8	2650	1.32	- Z_{max} was aligned with the outlet keys for studied weir geometries. - Z_{max} for rectangular model is higher than trapezoidal model for similar hydraulic conditions - Scour depth near outlet key 13% greater than inlet key
Lantz et al. (2021)	Type A PKW	*W*=1.94 m *P*=0.42 m *L/W*= 5.2	*Q*= 150-600 l/s *Q/W*= 0.077-0.309 m^2/s *Hu/P*=0.11-0.35	Up to 1170 min	13 6.5	2604 2645	1.54 1.3	- Empirical formula characterizing toe scour with use of Apron as protection measure - $Z^A_{max} = Z_{max}\left\{1 - 0.01\left[(-2.8\ Fr_{d90} - 6.3)\left(\frac{La}{P}\right)^2 + (2.8Fr_{d90} + 64.9)\left(\frac{La}{P}\right)\right]\right\}$
Chooplou et al. (2022)	Type A PKW	*W*=0.75 m *P*=0.2 m *L/W*= 4.4	*Q*= 40-60 l/s *Q/W*= 0.053-0.08 m^2/s *Hu/P*=0.2-0.3	300 min	2.2	2650	NA	- Empirical formula characterizing toe scour features i.e., depth, location and length as Ψ - $\frac{\Psi}{P} = k\left(Ln\left(\frac{t}{t_e} + a\right)\right)^b\ (Fr_{d50})^c\left(\frac{\Delta Z}{P}\right)^d$
Chooplou et al. (2022)	Type A TPKW	*W*=0.75 m *P*=0.2 m *L/W*= 2.5	*Q* = 30-40 l/s *Q/W*= 0.04-0.053 m^2/s *Hu/P*=0.23-0.29	300 min	2.2	2650	NA	- Effect of TW level on scour, h_d/P increase leading decrease in toe scour
Kumar and Ahmad (2022)	Type A PKW Triangular nose	*W*=0.39 m *P*=0.11 m *L/W*= 4.9	*Q* = 30-40 l/s *Q/W*= 0.04-0.053 m^2/s *Hu/P*=0.23-0.29	300 min	2.2	2650	NA	- Empirical formula characterizing toe scour with and without apron - $\frac{Z_{SM}}{y_t} = 0.114\ (F_D)^{1.84}\left(\frac{\Delta H}{y_t}\right)^{0.94}\left(\frac{L}{W}\right)^{2.26}$ - $\frac{Z_{ASM}}{y_t} = 53.70\ (F_D)^{1.24}\left(\frac{L_A}{y_t}\right)^{-0.28}\left(\frac{y_t}{d_{50}}\right)^{-1.43}$
Lantz et al. (2022)	Type A PKW	*W*=1.94 m *P*=0.42 m *L/W*= 5.2	*Q* = 150-600 l/s *Q/W*= 0.077-0.309 m^2/s *Hu/P*=0.11-0.35	Up to 1170 min	13 6.5	2604 2645	1.54 1.3	- Hydraulic conditions and tailwater level affect scour mechanism and equilibrium morphology. - Estimate time evolution and maximum scour depth, location and scour length.

Karimi et al., (2023)	Type A PKW Arced PKW	W=0.726 m P=0.17 m L/W= 3.2 RPKW 3.6 Arced PKW	Q = 7-58 l/s Q/W = 0.009-0.08 m^2/s	NA	1.25 8.9	NA NA	NA NA	- Empirical formula characterizing toe scour features - $\frac{Z_{SM}}{H_u} = 1.746 \left(\frac{H_u}{P}\right)^{-0.296} \left(\frac{h_c}{P}\right)^{-0.236}$ - $\frac{X_{SM}}{H_u} = 1.081 \left(\frac{H_u}{P}\right)^{-0.162} \left(\frac{h_c}{P}\right)^{-0.108}$
Rdhaiwi et al. (2023)	Type C TPKW	W =0.6 m P =0.2 m L/W = 4.3	Q = 30-40 l/s Q/W= 0.05-0.067 m^2/s	NA	1.25 8.5	NA NA	1.294 1.26	- Decrease in scour depth with use of stilling basin
Bodaghi et al. (2024)	Type A TPKW	W =0.75	Q = 30-70 l/s Q/W= 0.04-0.093 m^2/s	300 min	2.2	NA	1.43	- Scour hole parameters were more pronounced under free flow conditions compared to submerged flow. - Increasing particle Froude number enhanced the geometric features of the scour hole
Chooplou et al. (2024)	PKW TPKW TrPKW	W =0.75 P =0.2 L/W= 5 RPKW, 4.4 TPKW, 4 TrPKW	Q =30-60 l/s Q/W=0.04-0.08 m^2/s		7.1 2.2	2677 2632	1.32 1.42	- Scour hole characteristics affected highly by PKW geometry, Froude number and tailwater depth. - Scour bed topography are more symmetric for rectangular PKW with asymmetry index getting higher for trapezoidal and highest for triangular PKW.
Fathi et al. (2024)	Type A TPKW Stepped outlet	W =0.75 P =0.2	Q = 30-60 l/s Q/W=0.04-0.08 m^2/s	180 min 300 min	7.1 2.2	2677 2632	1.32 1.42	- Scour hole characteristics for stepped outlet in trap PKW - Maximum scour depth was lower for the PKW with steps compared to PKW without steps - Toe scour was minimum for outlets with 10 steps with reduction of about 21% of scour index values